POLITECNICO DI TORINO
Repository ISTITUZIONALE

Hierarchical bases for non-hierarchic 3Dtriangular meshes

Terms of use:

Publisher copyright

(Article begins on next page)

20 April 2024

Hierarchical Bases for Nonhierarchic 3-D Triangular Meshes

Francesco P. Andriulli, Francesca Vipiana, *Member, IEEE*, and Giuseppe Vecchi, *Senior Member, IEEE*

Abstract—We describe a novel basis of hierarchical, multiscale functions that are linear combinations of standard Rao-Wilton-Glisson (RWG) functions. When the basis is used for discretizing the electric field integral equation (EFIE) for PEC objects it gives rise to a linear system immune from low-frequency breakdown, and well conditioned for dense meshes. The proposed scheme can be applied to any mesh with triangular facets, and therefore it can be used as if it were an algebraic preconditioner. The properties of the new system are confirmed by numerical results that show fast convergence rates of iterative solvers, significantly better than those for the loop-tree basis. As a byproduct of the basis generation, a generalization of the RWG functions to nonsimplex cells is introduced.

Index Terms—Antennas, hierarchical bases, method of moments (MoM), multiscale, multiresolution (MR) techniques, wavelets.

I. INTRODUCTION

IN THIS WORK WE present a new multiresolution (MR) basis for the analysis of a fully arbitrary 3–D conductor via the electric-field integral equation (EFIE) and the method of moments (MoM). The fully arbitrary geometry of the (possibly curved) conductor is discretized with (planar) triangular cells, and the MR basis is constructed as a linear combination of the Rao-Wilton-Glisson (RWG) functions [1] defined on the mesh.

We significantly extend here the work previously described in [2]–[4]. The previous MR scheme starts by generating a coarse mesh of the structure to be analyzed; i.e., the user needs to specify in the meshing process that the cells are significantly larger than usually employed for an accurate solution. The MR generation algorithm proceeds with subsequent bisection of the edges, until the cells reach the size desired for an accurate description of the problem; this last, finest mesh is called the "pixel" mesh. This generates a hierarchical set of nested meshes with different spatial scales and a likewise hierarchical set of RWG bases [2]–[4]; the actual MR basis is finally generated with operations on all of these meshes and associated RWG.

The MR generation scheme described here produces a MR basis starting from *any* mesh, and in a way totally transparent to the user. The MR basis has the same theoretical properties as the previous one, and essentially the same performance; in particular it has the ability to control conditioning and to accelerate the convergence of iterative solvers. Because the MR functions are expressed as linear combination of the RWG functions of the original mesh, use of the MR basis amounts in practice to an algebraic transformation of the MoM matrix, that allows its use to improve the convergence of iterative fast methods, as shown in [5]. The basis is built upon a sequence of meshes that inherit the hierarchic property of the mesh sequence defined in [2] and [3]; because the initial mesh does not conform to any further restriction (as it did in [2] and [3]), it will be shown that one needs to generalize the concept of meshes and associated RWG functions to nonsimplex cells.

To the best of the authors' knowledge, this paper is the first to present a MR basis for a completely general mesh of flat triangular facets discretizing a likewise fully arbitrary body. Also, the need to define a multilevel system of vector bases on meshes with nonsimplex cells will lead to a generalization of the RWG functions that is likely to be applicable also to endeavors different from the present one of constructing a MR system of vector basis functions.

In this paper, we will concentrate the analysis of the performance of the method on the case of dense meshes, i.e., on complex geometries with a large number of unknowns per wavelength, and/or disparate mesh cells sizes, and/or low frequency. These are typical occurrences in antennas, circuits, and packaging problems (e.g., [6]), or in scattering from complex, resonant structures like in frequency selective surfaces (FSS) and reflectarrays. In these cases geometrical details generate a fine mesh with respect to the wavelength; the condition number and/or the convergence speed of iterative solvers quickly degrade when complexity increases, or when the frequency decreases.

MR in MoM was traditionally conceived as a means of making a low-frequency MoM matrix sparse upon thresholding (e.g., see the literature cited in [2]). Our main emphasis here will be on the ability of the MR approach to act as an efficient preconditioner, and especially so for dense-mesh problems, so as to be an ideal companion to fast iterative solvers (as already shown in [5]). The reasons why this type of MR can positively act on the spectrum of the MoM matrix is the subject of a different work [7], [8].

Because of the advances proposed in this paper, the MR is transparent to the user. From the purely functional point of view, it can be used in fast MoM codes as if it were an algebraic precoditioner; yet, its effects are obtained by the way it handles geometry and the EFIE underlying physics.

Preliminary results of this paper were presented in the conference paper [9].

The paper is organized as follows: Section II reviews the necessary background, including previous work on the subject;

Section III describes the new hierarchical basis; Section IV presents numerical results that confirm the effectiveness of the proposed formulation, and Section V contains the conclusions.

II. BACKGROUND

A. EFIE-MoM Setting

We will be concerned with the Electric Field Integral Equation (EFIE) for a PEC body whose surface is denoted by Γ. The background medium may be either homogeneous or an infinitely extended layered dielectric. The surface Γ is discretized by a mesh with triangular cells, over which a usual system of Rao-Wilton-Glisson (RWG) $\vec{f}_i^{RWG}$ is defined. The unknown current $\vec{J}(\vec{x})$ is approximated by the above set of RWG basis functions; a Galerkin testing is used to convert the EFIE into the MoM linear system.

It is known that the EFIE-MoM system suffers from poor conditioning when the cell size is small with respect to the wavelength, and/or the frequency is low (e.g., see [10]). In particular, the EFIE is ill-conditioned at nearly zero frequency due to the decoupling of the electric and magnetic field [10]–[16]. The solution to the low frequency instability is to separate the solenoidal part of the current from the nonsolenoidal part in the solution process. The classical bases presented in literature to do this are the "Loop-Star" (LS) basis and the "Loop-Tree" (LT) basis [13]–[16].

However, the separation of the solenoidal part is not always enough to obtain a fast-convergent MoM solution (as required in fast MoM methods). To obviate this loss of efficiency, an algebraic preconditioner is adopted in [12] in association with a Loop-Star scheme. An efficient alternative basis for the nonsolenoidal part is proposed in [10]. Seen under this perspective, the MR approach presented in [2]–[4] also naturally introduces an alternative basis for the nonsolenoidal part (they also do so for the solenoidal part). That approach was introduced for triangular meshes with some restrictions, as detailed in the next subsection. It was shown to be very efficient in producing low condition numbers and fast convergence for dense-mesh problems.

B. MR on Hierarchical Mesh Families

In order to better understand the present MR basis and its novelty, it is useful to recall the generation procedure and properties of the MR basis described in [2], [3]. The initial step of the method was the creation of a multilevel system of sets of basis functions of increasing fineness, i.e., with an increasing number of basis functions of increasingly smaller spatial support; each set of basis functions is described exactly by linear combinations of the basis functions of the sets of finer basis functions. The underlying geometrical operation is the generation of a family of meshes of increasing fineness; the starting mesh is as coarse as compatible with geometry; the second and further (finer) meshes are obtained by subsequent halving of the edges of the preceding mesh. By doing so, each cell of a given mesh includes exactly an integer number of cells belonging to finer meshes. A family of meshes with this property is termed "hierarchical". On this specific class of hierarchy all cells of all
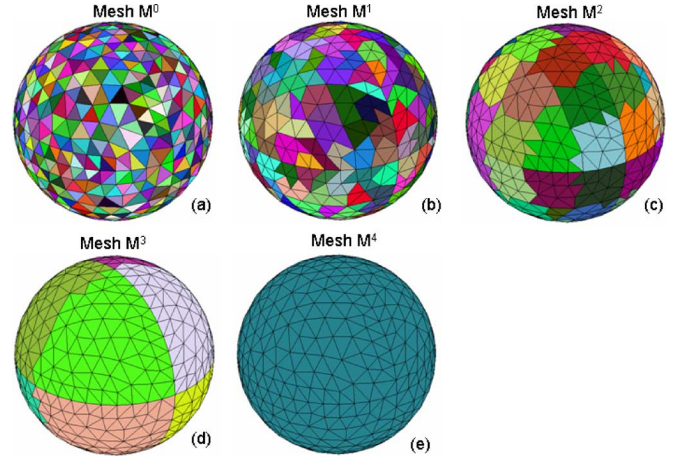

Fig. 1. Oct-tree subdivision of the cells.

meshes are triangular, and on each of them one can naturally define continuous-normal linear-tangential (CNLT) basis functions, i.e., Rao-Wilton-Glisson (RWG) functions; as shown in [4] the RWG of each mesh can be expressed exactly as linear combinations of the RWG defined on finer meshes. This is a key ingredient of the scheme devised in [2], [3], that significantly eases the creation of the MR basis. We remark that the collection of all RWG on all levels constitutes a redundant set; the actual (nonredundant) MR basis is be derived from this redundant set. This scheme can be framed in the general hierarchical decomposition of spaces summarized in Appendix A.

III. FORMULATION

In the new scheme, one starts with the usual mesh that discretizes the considered structure with the required accuracy [see, e.g., Fig. 1(a)].

The new hierarchical basis will keep the separation between the nonsolenoidal and the solenoidal part as in [2]–[4] (refer to Section II). Two separate bases will be constructed, for each of the two parts, using different techniques and finally joined together to obtain the complete basis set.

Because of the way it proceeds, the mesh-bisecting-based algorithm in [2] and [3] will be termed here "Top-down." By contrast, here we will start from the finer mesh, and proceed to generate coarser meshes in a generalized sense. Hence, the present approach will be called "bottom-up" generation.

A. Hierarchical Generalized Meshes

Our input is an arbitrary triangular mesh. There are no constraints to the mesh properties (including curvature) or to the topology of the structure under consideration: this is the mesh one would usually generate and employ to obtain a solution with the desired accuracy.

The first step of the MR algorithm is the generation of a hierarchical family (set) of meshes, to be effected starting from the input triangular (nonhierarchical) mesh. We denote this initial mesh with M^0, and call it level-0 mesh. All other meshes will be composed of groups of adjacent cells of the initial mesh, that we will call "macro-cells." Hence, the initial mesh M^0 will be the finest mesh of the family.

We start by considering groupings of adjacent cells in M^0 formed so that their average area is about four times the average area of the cells in M^0 (the aggregation process is described later), as in the example in Fig. 1(b). The union of these "macro-cells" forms a covering of the structure made up of nonsimplex cells, i.e., neither triangular nor quadrilateral. This covering will be called "generalized mesh" of level-1, M^1. The same procedure applied to M^1 will generate the generalized mesh M^2, and so forth until a level L where the generalized mesh M^L contains a single macro-cell covering the entire structure [refer to Fig. 1(e)]. It is apparent that this set $\{M^l, \quad l = 1, \ldots, L\}$ of generalized meshes is hierarchical in the sense defined in Section II-B. We warn the interested reader that the numbering of levels here is reversed with respect to that in [2]–[4]; this is due to the fact that this is a bottom-up geometrical process, as opposed to the top-down one of [2]–[4].

The most direct way of obtaining the mesh hierarchy is based on the well-known oct-tree algorithm (e.g., see [17]). The related grouping procedure has two steps, which will be described with the help of Fig. 1.

First, we apply the oct-tree grouping to the initial mesh (M^0), sequentially generating the partitions labelled $e, d, \ldots, a$ in Fig. 1. The algorithm stops when all partitions are either empty or comprised of only one (standard) cell of M^0.

Next, we define the other meshes of the hierarchical family proceeding in reversed order. The $L-$ level mesh M^L is composed of one macro-cell only, constituted by the union of all the (standard) cells of initial mesh M^0; the mesh M^{L-1} has at most eight macro-cells, and so forth until mesh M^0, as shown in the example in Fig. 1.

We observe that the appearance of nonsimplex (macro) cells is not a problem of the oct-tree algorithm; no grouping algorithm can avoid this situation, since the hierarchy of meshes is generated bottom up from an unrestricted mesh, and not vice-versa by bisections of an initial coarse mesh.

In the next sections, we will generate a set of vector basis functions on these generalized meshes, with the further constraints that they must form a hierarchy, and that these basis functions must be expressible as linear combinations of the RWG of the initial M^0 mesh. This is a key issue of our procedure; as far as we know, this has never been addressed before.

On the other hand, the grouping algorithm is immaterial to the present key issue of generating a basis on the nonsimplex meshes of our hierarchy. The oct-tree algorithm will not generate optimized groupings on complex topologies, where *ad-hoc* and more sophisticate grouping algorithms can outperform it. However, because it is well known and widespread in hierarchic grouping problems we will imply it in our description.

Summing up the mesh hierarchy generation, we will have a set of generalized meshes, each formed by nonsimplex macro-cells, that are the generalization of the cells of a standard mesh; the piecewise-straight curve shared by two adjacent macro-cells constitutes a generalized edge.

The nonsimplex (macro) cells of the generalized meshes will be denoted by the symbols c_n^l, where $l = 1, \ldots, L$ denotes the level of the mesh to which the cell belongs and n runs over all the (macro) cells of the $l-$ level mesh.

In order to simplify language, in the following we will drop the term "generalized" in mentioning generalized meshes and their generalized cells and edges wherever the distinction with respect to standard meshes, cells and edges is not necessary.

B. Nonsolenoidal Basis

The nonsolenoidal hierarchical basis will be obtained constructing first a scalar hierarchical basis. Then a proper scalar-to-vector operator will transform the scalar basis into the desired nonsolenoidal (vector) hierarchical basis; this is the subject of Section III-B.II. This way of proceeding will allow to prove that the obtained vector basis is a hierarchical decomposition (refer to Appendix A) and, simultaneously, it will give a practical way to generate the hierarchical basis.

As discussed earlier in [13], the nonsolenoidal current can be put in correspondence with its divergence, which is the surface charge. Our procedure can then be thought as a two-step one in which a basis is first constructed for the charge, and then relating it back to the current. In doing so, the scalar basis has to conform to the constraint that it be a valid charge for dynamic currents, i.e., it has to have zero average.

1) A Scalar Hierarchical Basis: We will construct our hierarchical scalar basis on the hierarchical family of meshes described previously.

Consider any level-l mesh M^l; on this mesh we define the space X_C^l of the zero-average functions that are piecewise constant on the M^l cells ($l = 1, \ldots, L$); as alluded above, in physical terms, they represent the charge associated to currents. Note that the mesh M^L is different from all others, since it contains a single cell (extending on the entire structure; see Fig. 1); as a result, the zero-average constraint cannot be met on it, and therefore it will be discarded, leaving $l \in [0, (L-1)]$.

In the following we describe a basis for the charge functions X_C^0 of the finest (i.e., standard) mesh that is a hierarchical decomposition (in the meaning defined in Appendix A). Following the standard practice in defining hierarchical bases, we will inductively describe how to obtain a basis for the space of level $l - 1$ (l arbitrary) assuming the basis of the space of level l as given. Specifically, from the basis of X_C^l the basis for X_C^{l-1} will be obtained.

For each pair of adjacent level-$(l-1)$ cells c_h^{l-1}, c_k^{l-1} of areas A_h^{l-1} and A_k^{l-1}, define the functions $\psi_j^l(\vec{x}) \in X_C^{l-1}$

$$\psi_j^l(\vec{x}) = \begin{cases} \frac{1}{A_k^{l-1}} & \vec{x} \in c_k^{l-1} \\ -\frac{1}{A_h^{l-1}} & \vec{x} \in c_h^{l-1} \\ 0 & \text{otherwise} \end{cases} \qquad (1)$$

where the index k in c_k^{l-1} runs from zero to the number of cells in M^{l-1} and j from zero to the number of pairs of adjacent cells in M^{l-1}, i.e., the number of inner edges in M^{l-1}. Note that the above is the generalization of the charge of a RWG function to pairs of nonsimplex cells; an example is shown in Fig. 2.

Now, for each cell $c_k^l \in X_C^l$, consider the cells $c_{h(k)}^{l-1} \in X_C^{l-1}$ *completely included* in c_k^l, and define G their number. Define the functions $\psi_{j(k)}^l$ between all the pairs of cells $c_{h(k)}^{l-1}$ as outlined
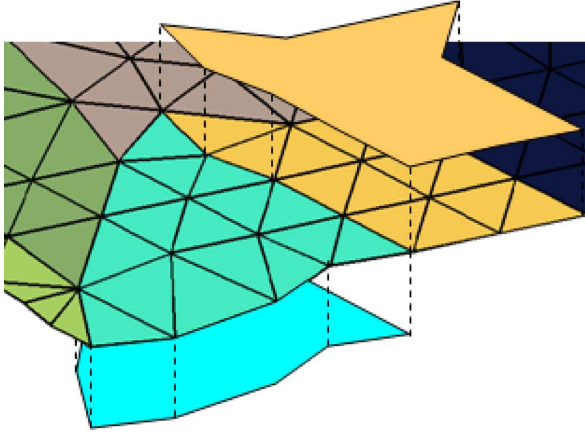
Fig. 2. Example of generalized charge function ψ.

by (1); note that the domain of these functions $\psi^l_{j(k)}$ will be completely included in the cell c^l_k. Let F be the number of these functions; in the following for the sake of cleanness the index $j(k)$ in $\psi^l_{j(k)}$, will be substituted by $f = 1, \ldots F$.

Recalling that the functions ψ^l_j are constant on each cell of M^l, define the matrix $\boldsymbol{Q}^l_k \in \mathrm{R}^{G \times F}$ as

$$\left[\boldsymbol{Q}^l_k \right]_{g,f} = \psi^l_f(\vec{x}) \big|_{c^l_g}. \tag{2}$$

For arbitrary topologies of Γ, the matrix $\boldsymbol{Q}^l_k$ is always rectangular ($G < F$); equivalently, the functions $\psi^l_f(\vec{x})$ are not linearly independent. Using a rank-revealing-QR decomposition [18], a subset $\{\psi^l_{f(i)}(\vec{x})\}$, $i = 1 \ldots, \mathrm{rank}(\boldsymbol{Q}^l_k)$ of the functions $\{\psi^l_f(\vec{x})\}$ is extracted; this can be repeated for all the cells of M^l (i.e., k running from zero to the number of cells in M^l). Defining now

$$W^l = span \left\{ \bigcup_k \{\psi^l_{f(i)}(\vec{x})\} \right\} \tag{3}$$

we obtain the basis for X^{l-1}_C as

$$X^{l-1}_C = X^l_C \oplus W^l \tag{4}$$

where $\oplus$ is the "direct sum" operator [inter alia, it is defined via (17) and (18)]. The procedure can be iterated till the level 0, obtaining

$$X^0_C = X^L_C \oplus \bigoplus_{n=1}^{L} W^n = \bigoplus_{n=1}^{L} W^n \tag{5}$$

which is the desired hierarchical decomposition of X^0_C [the last equality in (5) follows form the fact that X^L_C is empty].

2) Scalar-to-Vector Operator and Hierarchical Basis of the Nonsolenoidal Space: In the following, we will construct the

operator $\mathcal{A}$ which maps the scalar functions defined in the previous section onto the vector space of the nonsolenoidal currents. The analytic definition of this operator is possible, but not straightforward. Since it is not of interest in this context, we will opt for an operative and implementation-oriented definition. To this aim, consider a generic function $\psi^l_j(\vec{x})$ defined as in (1) on the pair of adjacent cells c^l_{j1} and c^l_{j2} belonging to M^l. It will be sufficient to define how the operator $\mathcal{A}$ acts on the scalar functions $\{\psi^l_j(\vec{x})\}$ to obtain the vector functions

$$\vec{f}^l_j(\vec{x}) = \mathcal{A}(\psi^l_j(\vec{x})). \tag{6}$$

In our operative approach, we will determine the coefficients that represent the sought-for vector function $\vec{f}^l_j(\vec{x})$ as a linear combination of the RWG functions of the finest (standard) mesh M^0.

The definition of $\mathcal{A}(\psi^l_j(\vec{x}))$ is recursive. Consider the functions $\{\psi^{l-1}_i(\vec{x})\}$ with domain completely included in the domain of $\psi^l_j(\vec{x})$ (i.e., in the union of c^l_{j1} and c^l_{j2}); their number N_{edg} is equal to the number of the edges internal to $c^l_{j1} \cup c^l_{j2}$. We define

$$\mathcal{A}(\psi^l_j(\vec{x})) = \sum_{i=1}^{N_{\mathrm{edg}}} \alpha_i \mathcal{A}(\psi^{l-1}_i(\vec{x})) \tag{7}$$

where α_i are coefficients to be determined. Note that the number of coefficients is equal to the number of internal edges N_{edg}. They can be determined setting a linear system of N_{edg} linearly independent equations. Let N_{cell} be the number of cells of the mesh M^{l-1} included in $c^l_{j1} \cup c^l_{j2}$. We can enforce

$$\nabla \cdot \vec{f}^l_j(\vec{x}) = \nabla \cdot \mathcal{A}(\psi^l_j(\vec{x})) = \psi^l_j(\vec{x}) \tag{8}$$

in each of these cells. In this way N_{cell} linear equations in the unknowns α_i are obtained; denote with $\boldsymbol{A} \in \mathrm{R}^{N_{\mathrm{cell}} \times N_{\mathrm{edg}}}$ the associated coefficient matrix. Euler theorem ensures that only $N_{\mathrm{cell}} - 1$ of them are linearly independent, so define the matrix $\tilde{\boldsymbol{A}} \in \mathrm{R}^{N_{\mathrm{cell}}-1 \times N_{\mathrm{edg}}}$ obtained deleting an arbitrary row from $\boldsymbol{A}$. The $(N_{\mathrm{edg}} - N_{\mathrm{cell}} + 1)$ missing equations for the coefficients α_i correspond to the null space of $\boldsymbol{A}$, that can be found from the SVD decomposition

$$\boldsymbol{A} = \boldsymbol{V} \boldsymbol{S} \boldsymbol{U}^T. \tag{9}$$

Consider the matrix $\tilde{\boldsymbol{U}}$ obtained deleting the columns of $\boldsymbol{U}$ corresponding to null singular values (if any) in $\boldsymbol{S}$. The coefficients α_i of the intermesh recursion in (7) will be obtained solving the linear system

$$\begin{bmatrix} \tilde{\boldsymbol{A}} \\ \tilde{\boldsymbol{U}}^T \end{bmatrix} \begin{pmatrix} \alpha_1 \\ \alpha_2 \\ \vdots \\ \alpha_{N_{\mathrm{edg}}} \end{pmatrix} = \begin{pmatrix} \psi^l_j(\vec{x}) \big|_{c_1} \\ \psi^l_j(\vec{x}) \big|_{c_2} \\ \vdots \\ \psi^l_j(\vec{x}) \big|_{c_{N_{\mathrm{cell}}}} \\ \hline \boldsymbol{0} \end{pmatrix}. \tag{10}$$
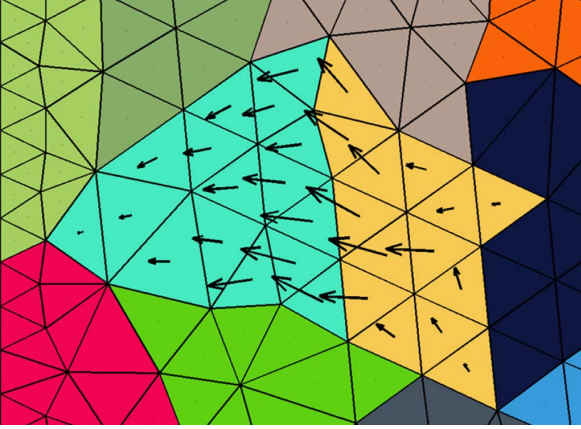
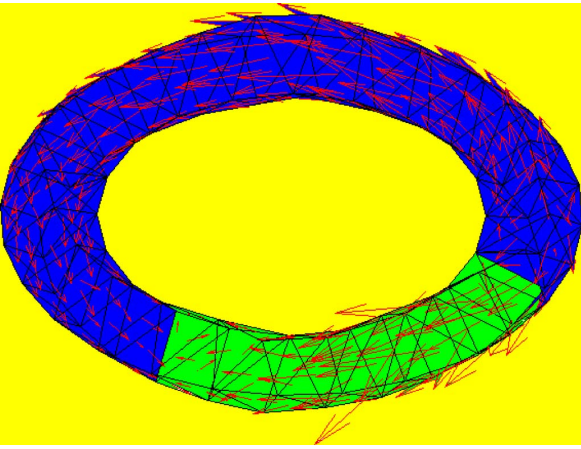Fig. 3. Example of a generalized RWG function defined on a pair of nonsimplex cells.

Fig. 4. Example of a generalized RWG function $\vec{f}_j^l(\vec{x})$ defined on the pair of nonsimplex cells seen in background with different colors. The segment corresponding to the defining edge of a RWG is the cell boundary on the right; the cell boundary on the right has no counterpart in standard RWG.

This scheme is applied recursively to $\mathcal{A}(\psi_i^{l-1}(\vec{x}))$, and the recursion terminates when the level 0 is reached; in this case we set

$$\mathcal{A}(\psi_i^0(\vec{x})) = \vec{f}_i^{RWG} \tag{11}$$

where $\vec{f}_i^{RWG}$ is the (unique) RWG function so that

$$\nabla \cdot \vec{f}_i^{RWG} = \psi_i^0(\vec{x}). \tag{12}$$

Note that the vector functions $\vec{f}_j^l(\vec{x})$ in (6), because of the definition of their corresponding charge in (1), constitute *generalized RWG* functions defined on pairs of nonsimplex mesh cells. Examples are shown in Figs. 3 and 4; the two figures show both a "direct" extension of the RWG (Fig. 3) and a case (Fig. 4) that has no direct counterpart in RWG functions.

The hierarchical basis of the nonsolenoidal space is now immediately obtained applying the operator $\mathcal{A}$ to all the functions $\{\psi_{f(i)}^l(\vec{x})\}$ (defined in the previous section) that constitute the scalar MR basis for the nonsolenoidal space.

Finally, note that the complexity of the SVD operations in (9) is low and independent of the size of the problem, i.e., of the

TABLE I
CASE OF A SPHERE MESHED WITH 4296 AND WITH 5988 UNKNOWNS, FOR EVERY LEVEL: MINIMUM, MAXIMUM, AND AVERAGE NUMBER OF SUBCELL PER CELL AND INTERNAL EDGES PER CELL

SPHERE ($N = 4296$)	Number of subcells per cell			Number of internal edges per cell		
Level	min.	max.	aver.	min.	max.	aver.
1	4	8	7	3	8	6
2	3	14	8	2	24	10
3	3	18	10	2	37	16
4	9	22	13	12	47	24
5	11	11	11	19	21	19

SPHERE ($N = 5988$)	Number of subcells per cell			Number of internal edges per cell		
Level	min.	max.	aver.	min.	max.	aver.
1	4	8	7	3	8	6
2	3	13	8	2	24	9
3	3	18	9	3	37	15
4	3	21	11	2	42	19
5	3	13	9	2	26	15
6	11	11	11	13	13	13

number of cells of the (standard) mesh M^0. This since, with the oct-tree subdivision algorithm, the number of subcells per cell (and thus the number of internal edges per cell) is approximately constant. This fact is verified in Table I where, for a sphere meshed with 4296 and 5988 unknowns, the number of internal edges per cell is reported against the level. Note that from the table it is evident that the number of internal edges per cell is approximately constant when varying the level and, most important, constant when increasing the number of unknowns. The concerned matrix is $\boldsymbol{A} \in \mathrm{R}^{N_{\text{cell}} \times N_{\text{edg}}}$, $N_{\text{edg}} < N_{\text{cell}}$, and N_{cell} is the number of cells of the mesh M^{l-1} that are included in a pair of adjacent cells of the mesh M^l; as explained in the mesh hierarchy construction in Section III-A, on average there are four level-$(l-1)$ cells in each level $-l$ cell, so the average value of N_{cell} is eight and independent on the size of the standard mesh M^0.

3) An Algorithmic Summary of the Procedure Leading to the Nonsolenoidal Hierarchical Basis: We will summarize now the entire procedure to obtain the nonsolenoidal hierarchical basis.

- Start from an arbitrary mesh (called "fine mesh" in the following);
- Group the cells of the fine mesh in macro-cells each of average area four times the average area of the cells of the fine mesh. A new mesh is obtained in this way;
- Recursively repeat the procedure obtaining a hierarchy of meshes the last of which is constituted by a single cell enclosing the entire structure;
- For each mesh of the hierarchy, for each cell of the mesh consider the functions ψ defined in (1) with domain completely included in the cell; select the linearly independent ones with a QR rank-revealing decomposition;
- For each linearly independent function ψ obtained at the previous point associate a "generalized RWG" obtained iterating between the expansion (7) and the system (10);
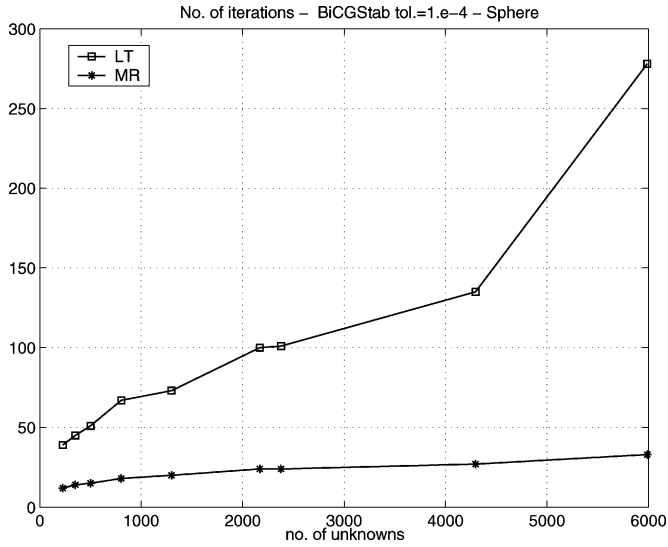
Fig. 5. Conducting sphere, with radius $= 1$ m, illuminated by a plane wave at the frequency of 1 kHz; number of iterations versus number of unknowns, BiCGStab solver with tolerance $= 10^{-4}$. Stars: MR, squares: LT.

- The set of all the generalized RWGs obtained in this way constitutes the nonsolenoidal basis.

C. Solenoidal Basis

We have observed that the use of a hierarchical decomposition of the nonsolenoidal part together with a non hierarchical loop basis suffices to obtain well-conditioned MoM matrices and fast convergent solvers (refer to Section IV). The same consideration can also be extracted from [10], that employs a standard loop basis for the solenoidal part.

However, for sake of symmetry, we will sketch here how a hierarchical decomposition of the solenoidal space can be obtained. It is sufficient to observe that in the *dual* mesh, every internal node will become a cell. As a consequence, a node-based loop basis will translate — on the dual mesh — into a patch basis set. Wavelets decompositions are known for such a function space. In particular the Generalized Haar basis [19] decomposes this space with sparse transformation matrices. It is sufficient to apply this Haar transformation matrix to the loop space, to obtain automatically the solenoidal hierarchical decomposition.

IV. NUMERICAL RESULTS

As test cases to verify the performance of the proposed MR basis we analyze a conducting sphere illuminated by a plane wave at very low frequency, the discone antenna depicted in Fig. 6, a ship with a monopole antenna placed on the top deck, as shown in Fig. 12, and finally we present a model of an aircraft with a fuelling device (Fig. 16). We have chosen these examples because they posses dense meshes and/or disparate mesh cell sizes, critical cases for the classical bases; these geometries also present curved portions that can be handled with the developed MR basis using flat triangular facets in the discretization without restrictions.

The MR basis is compared with the RWG [1] and Loop-Tree (LT) basis [15]. As performance indicators the 2-norm condition
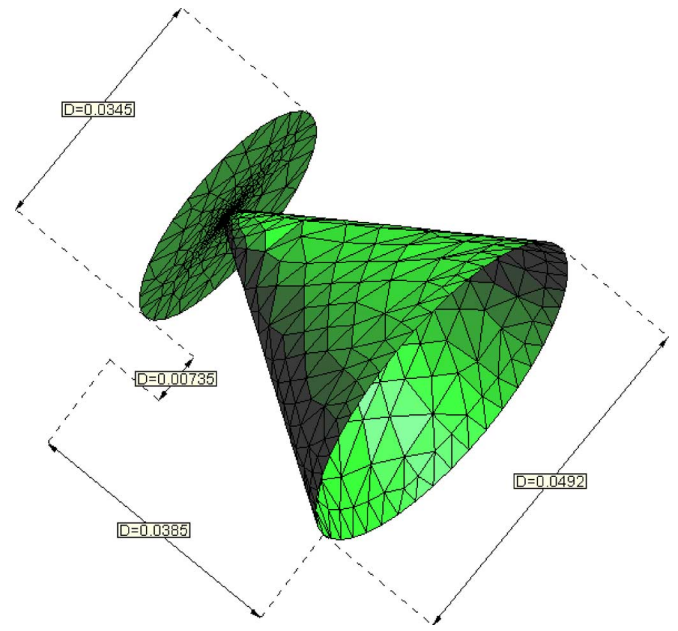

Fig. 6. Discone antenna: mesh, no. of unknowns $= 3469$; all the dimensions are in meters.
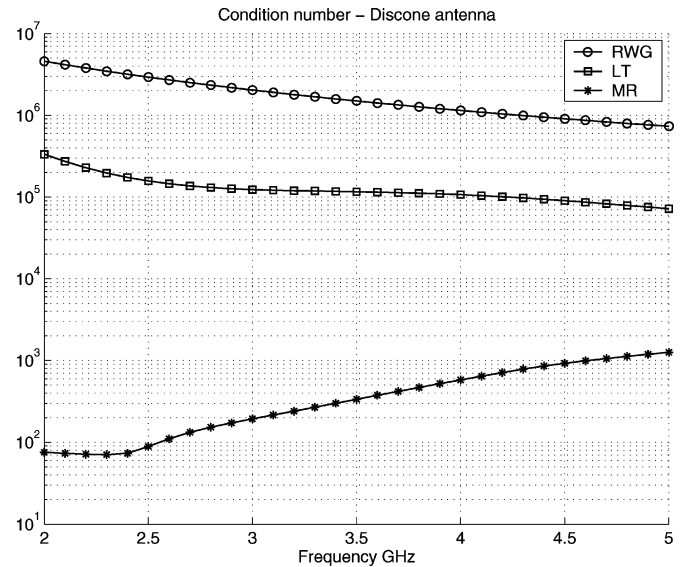

Fig. 7. Discone antenna: condition number versus frequency. Circles: RWG, stars: MR, squares: LT.

number is evaluated and the system is solved with the BiCGStab iterative solver [20] with tolerance equal to 10^{-4}. Finally, we remark that all the results with all the considered bases are obtained after the application of a diagonal preconditioning (DP) to the MoM matrix.

The PEC sphere has a radius of 1 m and is illuminated by a plane wave at the frequency of 1 kHz; this is an example at very low frequency where the scatterer is discretized with a dense and uniform mesh, as depicted in Fig. 1(a) (Mesh M^0). Fig. 5 shows the number of iterations to solve the system versus the number of unknowns; a faster convergence of the MR is evident with respect to the LT basis, especially with the increasing of the
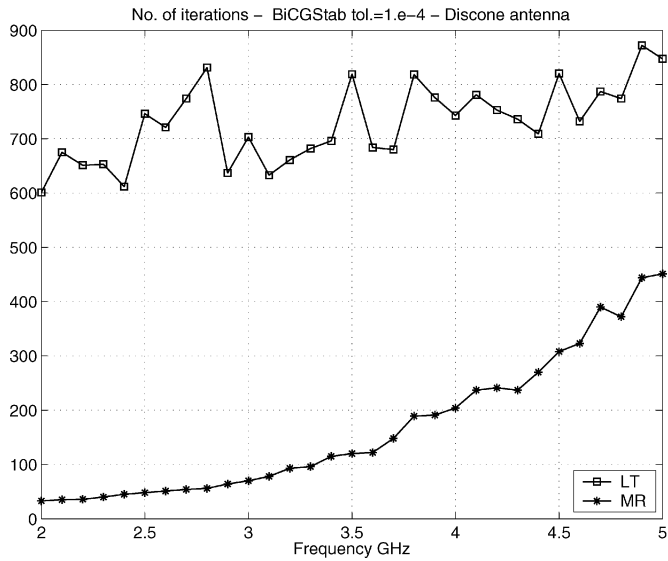
Fig. 8. Discone antenna: number of iterations versus frequency, BiCGStab solver with $\mathrm{tolerance} = 10^{-4}$. Stars: MR, squares: LT. For the RWG basis the solution is not reached in 4000 iterations.
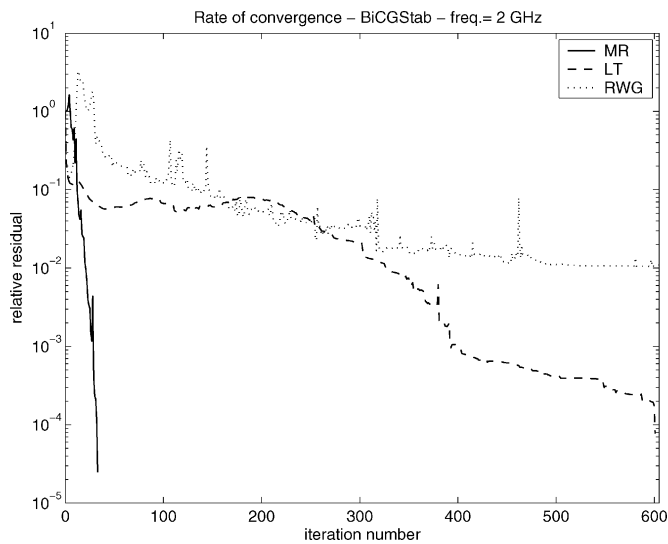

Fig. 10. Discone antenna $f = 2\,\mathrm{GHz}$. Relative error on the current by using different basis functions.

Fig. 9. Discone antenna $f = 2\,\mathrm{GHz}$. Convergence rate of the BiCGStab for different basis functions.

Fig. 11. Discone antenna, overall runtime (= Basis generation+ Basis change + Solution with BiCGStab, tol. = 10^{-4}) versus frequency, CPU time relevant to a Pentium IV 3.2 GHz.

number of unknowns. We do not report the results of the RWG basis because, as expected, the system does not converge.

The second example is a discone antenna discretized with 3469 unknowns, as shown in Fig. 6; it is excited by a voltage gap between the circular plate and the tip of the cone. The results show the condition number (Fig. 7) and convergence (Fig. 8) in the frequency band $2 - 5$ GHz. In this case rather disparate mesh cell sizes are present: the mesh close to the feeding point is much finer than in other parts of the antenna. The condition number of the MoM matrix, depicted in Fig. 7, is strongly reduced applying the MR basis with respect to the LT basis. This behavior is reflected in the convergence of the iterative solver, shown in Figs. 8 and 9, where the number of iterations with the MR basis is lower than with the LT basis especially in the lower part of the frequency band. To test the validity of the MR solution, the
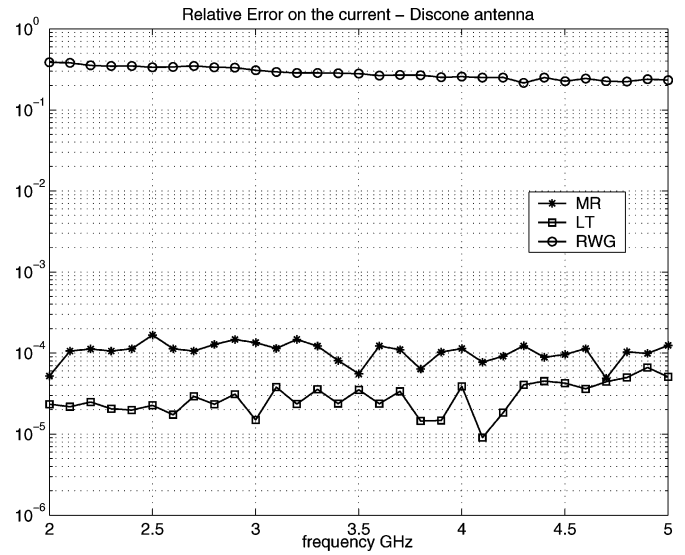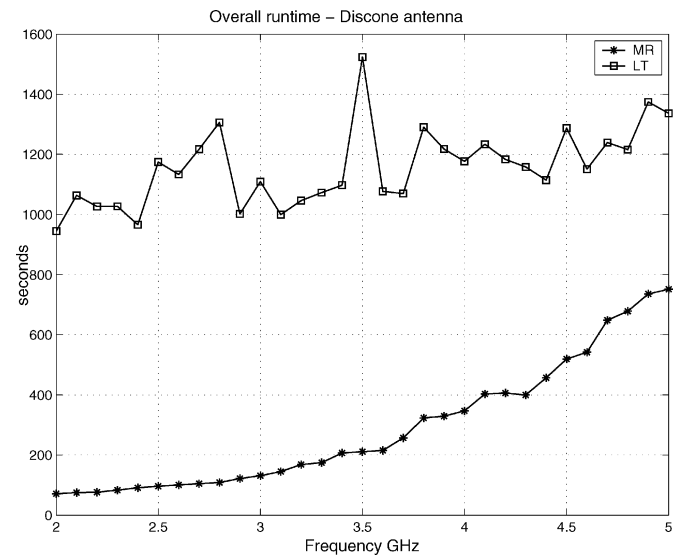
relative error obtained on the current by using the LT and MR basis is plotted in Fig. 10, the reference current has been obtained by direct inversion of the RWG impedance matrix. Note that the (iterative) RWG solution does not reach the prescribed accuracy (relative tolerance 10^{-4}) within 4000 iterations. The comparison of the CPU time necessary to obtain the solution using the LT basis and the MR basis is reported in Fig. 11. It is clear from the figure that a better behavior of the MR basis in terms of number of iterations translates in a better behavior in terms of CPU time.

The third example is an antenna placement that could be a critical case, especially at low frequencies, for the different mesh size between smooth surfaces and details of the antenna. The ship is PEC, and the monopole antenna is excited with a voltage gap at its base, where it connects to the ship surface.
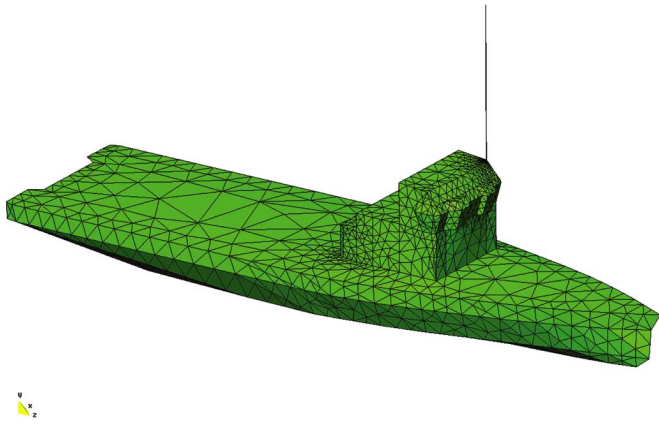
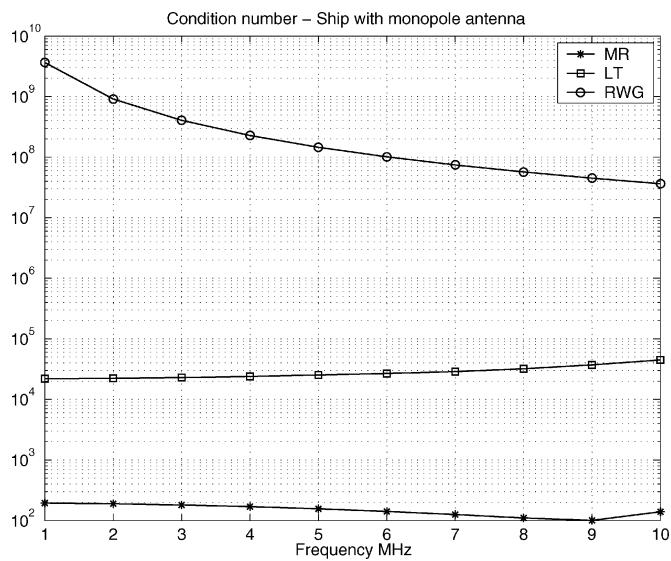Fig. 12. Ship with monopole antenna: mesh, no.of unknowns = 4442; the length of the ship is around 22 m.

Fig. 13. Ship with monopole antenna: condition number versus frequency. Circles: RWG, stars: MR, squares: LT.

Fig. 14. Ship with monopole antenna: no. of iterations versus frequency, BiCGStab solver with tolerance = 10^{-4}. Stars: MR, squares: LT. For the RWG basis the solution is not reached in 4000 iterations.

Fig. 15. Ship with monopole antenna, overall runtime (=Basis generation+ Basis change+Solution with BiCGStab, tol. = 10^{-4}) versus frequency, CPU time relevant to a Pentium IV 3.2 GHz.

The whole structure, shown in Fig. 12, is discretized with 4442 unknowns and analyzed from 1 to 10 MHz.

Fig. 13 shows the conditioning of the system and Fig. 14 the convergence of the solver: as in the previous cases using the MR basis we obtain a strong reduction of the condition number and a faster convergence with respect to the LT and RWG bases. The comparison of the CPU time necessary to obtain the solution using the LT basis and the MR basis is reported in Fig. 15. It is clear from the figure that the advantage of the MR basis in terms of number of iterations is reflected in an advantage in terms of CPU time.

The last test case is an aircraft (Fig. 16) with a highly discretized fuelling device. The aircraft is modelled as a PEC body, is excited with a plane wave of frequency $f = 1$ MHz coming from the top. The aircraft has been discretized with 20 532 RWGs, a low-frequency fast solver similar to the one in [21] has been used to compress the MoM matrix in this case. The edge length of the RWG functions on the aircraft's body is $\lambda/300$, while the edge length of the RWG functions on the fuel device (Fig. 17), which needs a finer discretization, is $\lambda/10000$. This
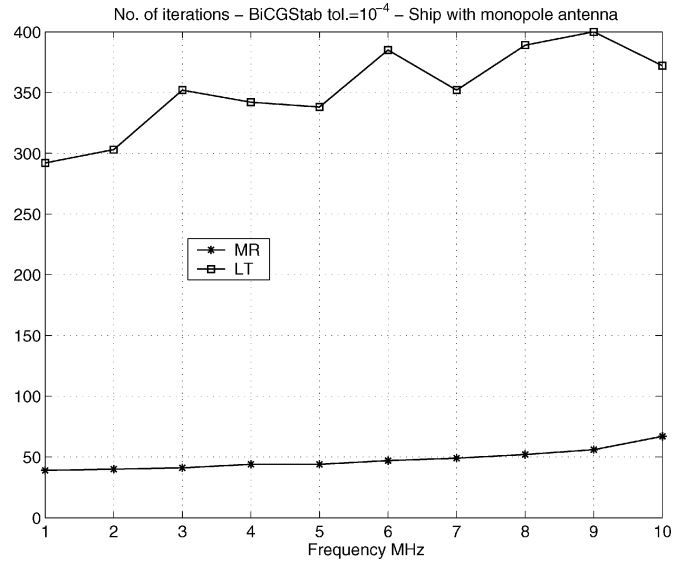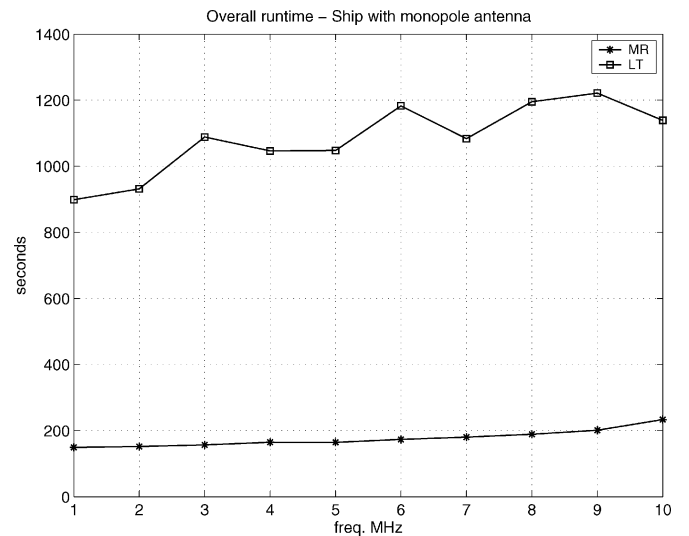
high difference in edge lengths will effectively test the capability of the MR basis of handling highly ill-scaled mesh problems. The absolute value of the simulated current with the MR basis is shown in Fig. 18. For this structure, the number of iterations and the CPU time for different basis functions are summarized in Table II; the advantages of using the MR are evident.

V. CONCLUSION

A novel set of hierarchical functions has been presented. When used to discretize the EFIE they give rise to a linear system which is immune from the low-frequency breakdown even in the presence of densely discretized meshes. The novel functions are expressed as linear combinations of the standard RWGs, and generated from a general triangular mesh without any restriction. Therefore, the change of basis from RWG to
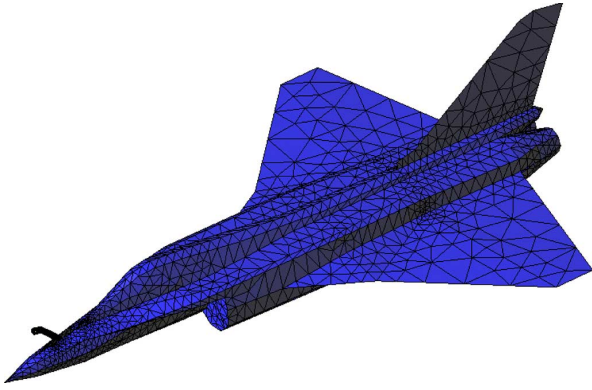
Fig. 16.   Aircraft: mesh, $\mathrm{no.\ of\ unknowns} = 20532$; the length of the ship is around 14 m.

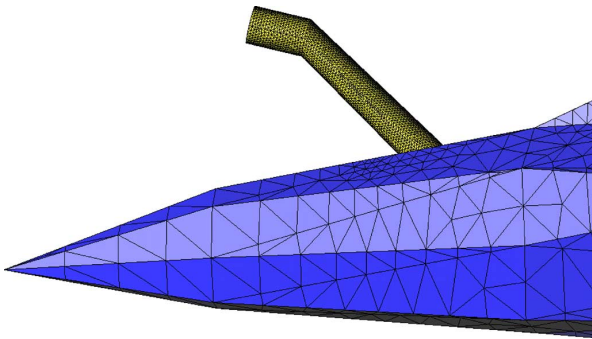Fig. 18.   Aircraft: absolute value of the current (dB).

Fig. 17.   Aircraft: detail of the fuel device.

the new basis can be used in practice as an algebraic preconditioner of the standard EFIE. Numerical results have shown the effectiveness of the proposed approach and its applicability to general structures of arbitrary topology.

APPENDIX

HIERARCHICAL DECOMPOSITIONS

This appendix reviews the abstract hierarchical decomposition of a function space.

The case described herein is more general than treated in the rest of the paper; this allows the interested reader to better frame the proposed method, and constitutes the logical background for possible extensions.

The description will be minimal and concise, the interested reader can find an exhaustive treatment of the subject in [22] and in the references therein.

General Hierarchical Decomposition: Consider a sequence of function spaces $X^i \quad i = 0, \ldots, L$ (with L fixed) satisfying

$$X^{i+1} \subset X^i. \tag{13}$$

For each i let $\phi_j^i \quad j = 1, \ldots, dim(X^i)$ be a basis of X^i. The basis functions ϕ_j^i were not used in Section III, but they may be necessary when using more general cases of cell groupings than described in Section III-B.I. An example of correspondence between these spaces and those spanned by the RWG functions is given at the end of the section.

TABLE II
RESULTS FOR THE AIRCRAFT DISCRETIZED WITH $N = 20532$ RWGs.

	Number of iterations to reach a relative tolerance of 10^{-6}	Overall runtime time relevant to a Pentium IV 3.2 GHz (hours)
Standard MOM	1990	77.42
Loop-Star	745	28.15
MR	92	5.23

For a given i, consider a linearly independent set of functions $\psi_j^i \quad j = 1, \ldots, (dim(X^{i-1}) - dim(X^i))$ so that the union set $\{\phi_j^i\} \cup \{\psi_j^i\}$ is a basis of X^i alternative to $\{\phi_j^{i-1}\}$ [22]. In other words

$$X^{i-1} = span(\{\phi_j^{i-1}\}) = span(\{\phi_j^i\} \cup \{\psi_j^i\}). \tag{14}$$

Defining

$$W^i = span(\{\psi_j^i\}). \tag{15}$$

Equation (14) can be rewritten as

$$X^{i-1} = X^i \oplus W^i. \tag{16}$$

This procedure can be iterated for $i = 0$ to $i = N$ obtaining

$$X^0 = X^L \oplus \bigoplus_{i=1}^{L} W^i \tag{17}$$

which is a hierarchical decomposition of X^0. Equation (17) can be rewritten in terms of bases as

$$\{\phi_j^0\} = \{\phi_j^L\} \cup \bigcup_{i=1}^{L} \{\psi_j^i\}. \tag{18}$$

Note that $\{\psi_j^i\}$ could be a subset of $\{\phi_j^{i-1}\}$; this is actually the case with the hierarchical basis functions presented in this

work. For the case employed in the rest of the paper, the correspondence between the general spaces and those employed is the following:

$$X^i = X^i_C, \quad W^i = span\{\psi^i_j\} \tag{19}$$

where the functions ψ^i_j are defined as in (1). As aforementioned, in the construction in Section III-B.I the functions ϕ^i_j are not present; this is due to the fact that $X^L_C = \{0\}$. In more general cell grouping schemes, where they can turn out useful, they can be defined as the divergence of the basis functions for the nonsolenoidal space, e.g., of the star or tree functions.

Decomposition via a Linear Operator Mapping: Given two function spaces X^i and Y^i and a bounded and invertible linear operator $\mathcal{A} : X^i \to Y^i$, assume a hierarchical decomposition of X^i as in (18). A hierarchical decomposition for Y^i is immediately obtained using the basis functions $\mathcal{A}(\phi^i_j)$ and $\mathcal{A}(\psi^i_j)$. Additional properties of the hierarchical basis of Y^i are ensured by this operation, but they are not of interest here. The details can be found in [4].

REFERENCES

[1] S. Rao, D. Wilton, and A. Glisson, "Electromagnetic scattering by surfaces of arbitrary shape," *IEEE Trans. Antennas Propag.*, vol. 30, pp. 409–418, May 1982.

[2] F. Vipiana, P. Pirinoli, and G. Vecchi, "A multiresolution method of moments for triangular meshes," *IEEE Trans. Antennas Propag.*, vol. 53, pp. 2247–2258, Jul. 2005.

[3] F. Vipiana, G. Vecchi, and P. Pirinoli, "A multiresolution system of Rao-Wilton-Glisson functions," *IEEE Trans. Antennas Propag.*, vol. 55, pp. 924–930, Mar. 2007.

[4] F. Andriulli, A. Tabacco, and G. Vecchi, "A multiresolution approach to the electric field integral equation in antenna problems," *SIAM J. Sci. Comput.*, vol. 29, pp. 1–21, Jan. 2007.

[5] P. De Vita, A. Freni, F. Vipiana, P. Pirinoli, and G. Vecchi, "Fast analysis of large finite arrays with a combined multiresolution SM/AIM approach," *IEEE Trans. Antennas Propag.*, vol. 54, pp. 3827–3832, Dec. 2006.

[6] W. C. Chew, L. J. Jiang, Y. H. Chu, G. L. Wang, I. T. Chiang, Y. C. Pan, and J. S. Zhao, "Toward a more robust and accurate CEM fast integral equation solver for IC applications," *IEEE Trans. Packaging*, vol. 28, pp. 449–464, Aug. 2005.

[7] F. Vipiana, P. Pirinoli, and G. Vecchi, "Regularization effect of a multiresolution basis on the EFIE-MoM matrix," in *Proc. IEEE Int. Symp. Antennas Propag.*, Washington , DC, Jul. 2005, vol. 3B, pp. 192–195.

[8] F. Vipiana, P. Pirinoli, and G. Vecchi, "Spectral properties of the EFIE-MoM matrix for dense meshes with different types of bases," *IEEE Trans. Antennas Propag.*, vol. 55, no. 11, pp. 3229–3238, 2007.

[9] F. P. Andriulli, F. Vipiana, and G. Vecchi, "Enhanced multiresolution basis for the mom analysis of 3D structures," in *Proc. IEEE Int. Symp. Antennas Propag.*, Honolulu, HI, Jun. 2007, pp. 5612–5615.

[10] J. S. Zhao and W. C. Chew, "Integral equation solution of Maxwell's equations from zero frequency to microwave frequency," *IEEE Trans. Antennas Propag.*, vol. 48, pp. 1635–1645, Oct. 2000.

[11] T. F. Eibert, "Iterative-solver convergence for loop-star and loop-tree decomposition in method-of-moments solutions of the electric-field integral equation," *IEEE Antennas Propag. Mag.*, vol. 46, pp. 80–85, Jun. 2004.

[12] J. F. Lee, R. Lee, and R. J. Burkholder, "Loop star basis functions and a robust preconditioner for EFIE scattering problems," *IEEE Trans. Antennas Propag.*, vol. 51, pp. 1855–1863, Aug. 2003.

[13] G. Vecchi, "Loop-star decomposition of basis functions in the discretization of EFIE," *IEEE Trans. Antennas Propag.*, vol. 47, pp. 339–346, Feb. 1999.

[14] M. Burton and S. Kashyap, "A study of a recent moment-method algorithm that is accurate to very low frequancies," *Appl. Computat. Electromagn. Soc. J.*, vol. 10, pp. 58–68, Nov. 1995.

[15] W. Wu, A. W. Glisson, and D. Kajfez, "A study of two numerical solution procedures for the electric field integral equation at low frequency," *Appl. Computat. Electromagn. Soc. J.*, vol. 10, pp. 69–80, Nov. 1995.

[16] D. R. Wilton, "Topological consideration in surface patch and volume cell modeling of electromagnetic scatterers," in *Proc. URSI Int. Symp. Electromagn. Theory*, Santiago de Compostela, Spain, Aug. 1983, pp. 65–68.

[17] W. C. Chew *et al.*, *Fast and Efficient Algorithms in Computational Electromagnetics*. Norwood, MA: Artech House Antennas Propag. Library, 2000.

[18] G. H. Golub and C. F. van Loan, *Matrix Computation*. Baltimore, MD: Johns Hopkins Univ. Press, 1989.

[19] T. von Petersdorff and C. Schwab, "Fully discrete multiscale Galerkin BEM," in *Multiscale Wavelet Methods for PDEs*. New York: Academic.

[20] H. A. V. der Vorst, "BI-CGSTAB: A fast and smoothly converging variant of BI-CG for the solution of nonsymmetric linear systems," *SIAM J. Sci. Stat. Comput.*, vol. 13, pp. 631–644, Mar. .

[21] K. Zhao, M. N. Vouvakis, and J.-F. Lee, "The adaptive cross approximation algorithm for accelerated method of moments computations of EMC problems," *IEEE Trans. Electromagn. Comp.*, vol. 47, no. 4, pp. 763–773, 2005.

[22] W. Dahmen, "Multiscale and wavelet methods for operator equations," *Multiscale Problems and Methods in Numerical Simulations*, vol. 31, no. 96, 2003.

Francesco P. Andriulli received the Laurea degree in electrical engineering from the Politecnico di Torino, Italy, in 2004, the M.S. degree in electrical engineering and computer science from the University of Illinois at Chicago in 2004, and the Ph.D. degree in electrical engineering from the University of Michigan at Ann Arbor, in 2008.

Since 2008, he has been a Research Fellow with the Politecnico di Torino. His research interests are in computational electromagnetics with focus on preconditioning and fast solution of frequency and time domain integral equations, integral equation theory, hierarchical techniques, integral identities, and single source integral equations.

Dr. Andriulli is the first prize recipient of the student paper competition at the 2007 URSI North American Radio Science Meeting and he has been awarded with the University of Michigan International Student Fellowship and with the University of Michigan Horace H. Rackham Predoctoral Fellowship.

Francesca Vipiana (M'07) received the Laurea and Ph.D. (Dottorato di Ricerca) degrees in electronic engineering from the Politecnico di Torino, Italy, in 2000 and 2004, respectively, with doctoral research carried out partly at the European Space Research Technology Centre (ESTEC, Noordwijk, The Netherlands).

Since 2004, she has been with the Electronics Department, Politecnico di Torino, as a Research Assistant. Her main research activities concern numerical techniques for antennas, circuits, and periodic structures analysis, and synthesis techniques for contoured-beam antennas.

Dr. Vipiana received the Young Scientist Award at the Union of Radio Science (URSI) General Assembly in 2005.

Giuseppe Vecchi (M'90–SM'07) received the Laurea and Ph.D. (Dottorato di Ricerca) degrees in electronic engineering from the Politecnico di Torino, Torino, Italy, in 1985 and 1989, respectively, with doctoral research carried out partly at Polytechnic University, Farmingdale, NY.

He was a Visiting Scientist at Polytechnic University from August 1989 to February 1990, when he joined Politecnico di Torino as an Assistant Professor (Ricercatore) in the Department of Electronics. From 1992 to 2000, he was an Associate Professor at Politecnico, and, since 2000 a Professor. He was a Visiting Scientist with the University of Helsinki, Finland, in 1992, and has been an Adjunct Faculty member with the Department of Electrical and Computer Engineering, University of Illinois at Chicago, since 1997. His main research activities concern analytical and numerical techniques for antennas and circuits analysis, RF plasma heating, antenna design for wireless communications, and electromagnetic compatibility.